Supplementary Information (SI) for Green Chemistry.
This journal is © The Royal Society of Chemistry 2025

Supporting information

NiFeCo Wrinkled Nanosheets Electrode for Selective Oxidation of 5-Hydroxymethylfurfural to 2,5-furandicarboxylic acid

Bingkun Chen[a], Bowen Yang[b], Yaqiong Su[c], Qidong Hou[b], Richard Lee Smith Jr[d], Xinhua Qi [b]*, Haixin Guo[a]*

[a]Agro-Environmental Protection Institute, Chinese Academy of Agricultural Sciences, No. 31, Fukang Road, Nankai District, Tianjin, 300191, China

[b]College of Environmental Science and Engineering, Nankai University, No. 38, Tongyan Road, Jinnan District, Tianjin, 300350, China

[c]GRIMAT Engineering Institute Co., Ltd., Beijing 104107, China

[d]Graduate School of Environmental Studies, Tohoku University, Aramaki Aza Aoba 468-1, Aoba-ku, Sendai, 980-8572, Japan

Corresponding author:

Email: haixin_g@126.com (HX), qixinhua@nankai.edu.cn (XH)

Section A. Synthesis of NiFeCo-LDHs catalysts

The hierarchical NiFeCo-LDHs nanosheet arrays catalyst was synthesized on nickel foam (NF) via a hydrothermal and subsequent oxidative activation (pyrolysis) method. For the preparation of hierarchical nanosheet arrays, $Ni(NO_3)_2 \cdot 6H_2O$, $Fe(NO_3)_3 \cdot 9H_2O$,

$Co(NO_3)_2 \cdot 6H_2O$ with a total amount of 0.6 mmol (Ni: Fe: Co = 3:1:2) and 1.0 mmol urea and 1.0 mmol NH_4F were ultrasonically mixed into 10 mL ultrapure water. The nickel foam was washed sequentially with 1M HCl, ethanol and ultrapure water to remove oxides, oil stains and residual HCl, and then vacuum dried at 60 ℃ for later use. The precursor solution was transferred into a 25 mL autoclave and a tablet of pre-cleaned NF (1×2 cm^2) was placed vertically into the vessel. Then, the autoclave was sealed and heated to 150 ℃ and maintained at reaction temperature for 6 h. The obtained solid material was washed with ethanol and ultrapure water, and then placed in a muffle furnace at a temperature of 300 °C for 2 h in the presence of air atmosphere, and finally the NiFeCo-LDHs hierarchical nanosheet arrays catalyst were obtained. The synthesis process mentioned above was followed to prepare NiFe-LDHs and NiCo-LDHs, NiFe-LDHs in the absence of $Co(NO_3)_2 \cdot 6H_2O$ and NiCo-LDHs and without the presence of $Fe(NO_3)_3 \cdot 9H_2O$ as given in the material names.

Section B. Materials and Characterization

Chemical reagents 5-hydroxymethylfurfural (HMF) (98%), 2,5-furandicarboxylic acid (FDCA) (98%), 2-formyl-5-furancarboxylic acid (FFCA) (98%), 5-hydroxymethyl-2-furancarboxylic (HMFCA) (98%), furan-2,5-dicarbaldehyde (DFF) (98%) were purchased from McLean (Shanghai, China). Metal nitrates, $Ni(NO_3)_2 \cdot 6H_2O$, $Co(NO_3)_2 \cdot 6H_2O$ and $Fe(NO_3)_3 \cdot 9H_2O$ and additives, urea (99.5%) and NH_4F (98%), were obtained from Aladdin (Shanghai, China). Nickel foam (NF) was obtained from Suzhou Sinero Company (Suzhou, China).

The crystal structure of the sample was studied on an Ultima IV X-ray diffractometer with Cu-K radiation (Rigaku Japan) in the sweep range of 10° to 90° with a scan speed of 8°/min. The morphology and structure features of the samples were characterized by

scanning electron microscopy (SEM, Japan Regulus 8100) with a working voltage of 10 kV with energy dispersion spectroscopy (EDS, Zeiss 500, Germany). Field-emission transmission electron microscopy (TEM, JEM 2100PLUS, Japan) used for observe the microstructures of samples. X-ray photoelectron spectroscopy (XPS) was conducted on a Escalab 250Xi with Al-K radiation and range correction was carried out using the binding energy of C 1s (284.8 eV) as the energy standard. Elemental analysis of the spent electrolyte was made with inductively plasma spectroscopy (Agilent, ICP-OES730). In situ fourier transform infrared spectroscopy (FTIR, Tianjin Nengpu iCAN 8 Plus) were collected in the range of (400 to 4000) cm^{-1}. In-situ Raman spectra were analyzed at difference potential using a Raman spectrometer (JINSP, RS2100 Lab).

Section C. Electrochemical measurements

Electrochemical performance of the electrode was evaluated with a CHI 660E electrochemical workstation (CH Instruments, Inc., Shanghai) in a three-electrode system at room temperature. The H-type electrolytic cell was separated by a Nafion 117 proton exchange membrane. The as-prepared samples electrode (1×2 cm^2), the saturated Ag/AgCl and carbon rod served as working and counter electrode, respectively. All the electrochemical oxidation experiments were performed in 30 mL of 1.0 M KOH (pH = 13.8) solution with 20/50 mM HMF. The measured potentials *vs* Ag/AgCl were converted to a reversible hydrogen electrode (*vs*. RHE) according to the Nernst equation (Formula 1). All linear sweep voltammetry (LSV) measurements were performed at a scan rate of 5 mV s^{-1} without IR compensation. Electrochemical impedance spectroscopy (EIS) tests were obtained over a frequency range of 0.1 Hz to 10^5 Hz. The Tafel slope was determined at a scan rate of 5 mV s^{-1}. Electrochemical surface area (ECSA) was calculated from the formula (2). Double-layer capacitance (C_{dl}) was evaluated using the cyclic voltammetry

(CV) curves recorded at scan rates of (20, 40, 60, 80, 100) mV s^{-1} in the non-Faraday region.

$$E\ (vs.\ \text{RHE}) = E\ (vs.\ \text{Ag/AgCl}) + 0.197\ \text{V} + 0.059 \times \text{pH} \quad (1)$$

$$\text{ECSA} = C_{dl} / C_s \quad (2)$$

where the C_{dl} value is obtained from CV curves at different scan rates, Cs is the specific capacitance of a flat smooth surface (F g^{-1}) and can be assumed to be 40 μF cm^{-2} according to the literature [1, 2].

Section D. Product analyses

The liquid was analyzed by high performance liquid chromatography (HPLC) (Waters e2489) with Aminex HPX-87H column at 35 ℃. H_2SO_4 (5mM) was used as the mobile phase with a constant flow rate of 0.6 mL/min. The detection wavelength of the UV detector was set at 210 nm. The qualitative and quantitative analysis of the sample was based on the retention time and standard curve of the standard samples. For each analysis, an aliquot of 1mL sample was extracted from the electrolytic cell and diluted 50 times with ultrapure water. Calibration curves were constructed to quantify HMF and its oxidation products. In this work, the HMF conversion, yields of the oxidation products and the faraday efficiency (FE) of the target FDCA were defined by the following formula.

$$\text{HMF conversion}\ (\%) = \left(1 - \frac{\text{moles of remaining HMF}}{\text{moles of initial HMF}}\right) \times 100\% \quad (3)$$

$$\text{FDCA yield}\ (\%) = \frac{\text{moles of FDCA formed}}{\text{moles of initial HMF}} \times 100\% \quad (4)$$

$$\text{FE}\ (\%) = \frac{\text{moles of FDCA formed} \times n \times F}{\text{total charge passed}} \times 100\% \quad (5)$$

where F is the Faraday constant (96485 C·mol^{-1}), and n is the theoretical number of electrons for oxidizing HMF to FDCA, which is 6.

Section E. Transfer coefficient (β) and turnover frequency (TOF)

$$\beta = \frac{2.303RT}{nbF} \tag{6}$$

where R, T, n, b and F are respectively gas constant (8.314 J/(K mol)), absolute temperature (K), number of electrons transferred, the Tafel slope and the Faraday constant (96485 C/mol).

$$TOF = \frac{JA}{6FN} \tag{7}$$

where J is the current density, A is the area of the electrode, 6 represents the number of transferred charges, F is the Faraday constant (96485C mol^{-1}), N indicates the mole number of the active metal sites. The quantity of N is calculated based on the data of ICP.

Section F. DFT calculations

Spin-polarized density functional theory (DFT) calculations were performed [3] with the Vienna ab initio 4/37 simulation package (VASP). The projector augmented wave (PAW) potentials within a generalized gradient approximation (GGA) was used to treat the exchange-correlation energy [4]. And PBE+U functional [5] with U-J of 5.5 eV applied on the d orbitals of Ni [6]. An energy cutoff of 400 eV was used. Bulk optimizations were performed for the system before their surfaces were cleaved. A k-point grid of 10×10×8, 2×2×1, and 3×3×1 was employed for the bulk β-$Ni(OH)_2$, the surfaces, and surfaces density of states calculations, respectively. All atomic positions were fully relaxed until energy and force reached the tolerance of 1×10−5 eV and 0.05 eV/Å, respectively.

Transition state TS was located by the dimer [7] method. The solvation effect was not included since the ignorable energy change was present. HMF adsorption energy E_{ads}(HMF) was defined as E_{ads}(HMF) = E_{total}(HMF/surface) – E_{total}(surface) – E_{total}(HMF). E_{total}(HMF/surface), E_{total}(surface) and E_{total}(HMF) are defined as the total energies of the optimized surface with adsorbed HMF, the optimized empty surface, and the optimized HMF molecule in the gas phase. Bulk β-Ni$(OH)_2$ was isostructural with brucite, with the space group P-3m1 and lattice parameters a = b = 3.127 Å and c = 4.606 Å [8]. A 4×4 unit cell of β-Ni$(OH)_2$-(001) surface was employed to perform the surfaces calculations and a vacuum region of 15 Å was adopted to separate periodic vertical images [9]. For HMF adsorption, the bonding modes via OH only, CHO only, both CHO and OH, and CH in the carbon ring on various sites were considered. The different removal sites for the dehydrogenation of models were also taken into account.

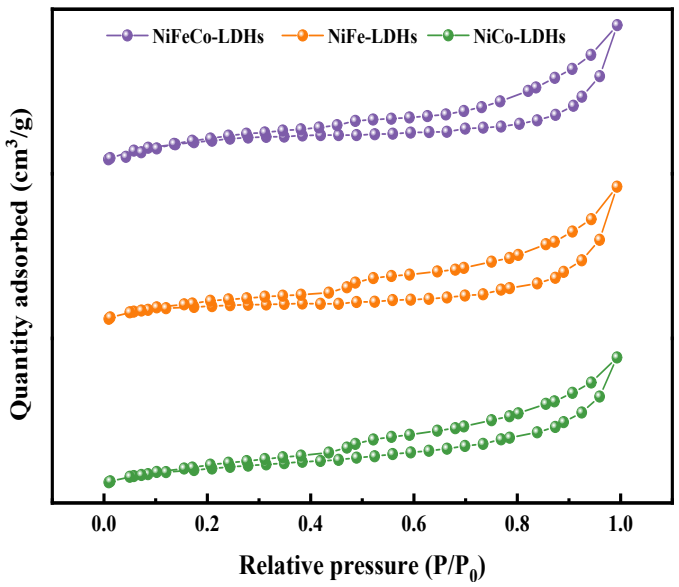

Figure S1. N_2 adsorption-desorption isotherms of prepared catalysts.

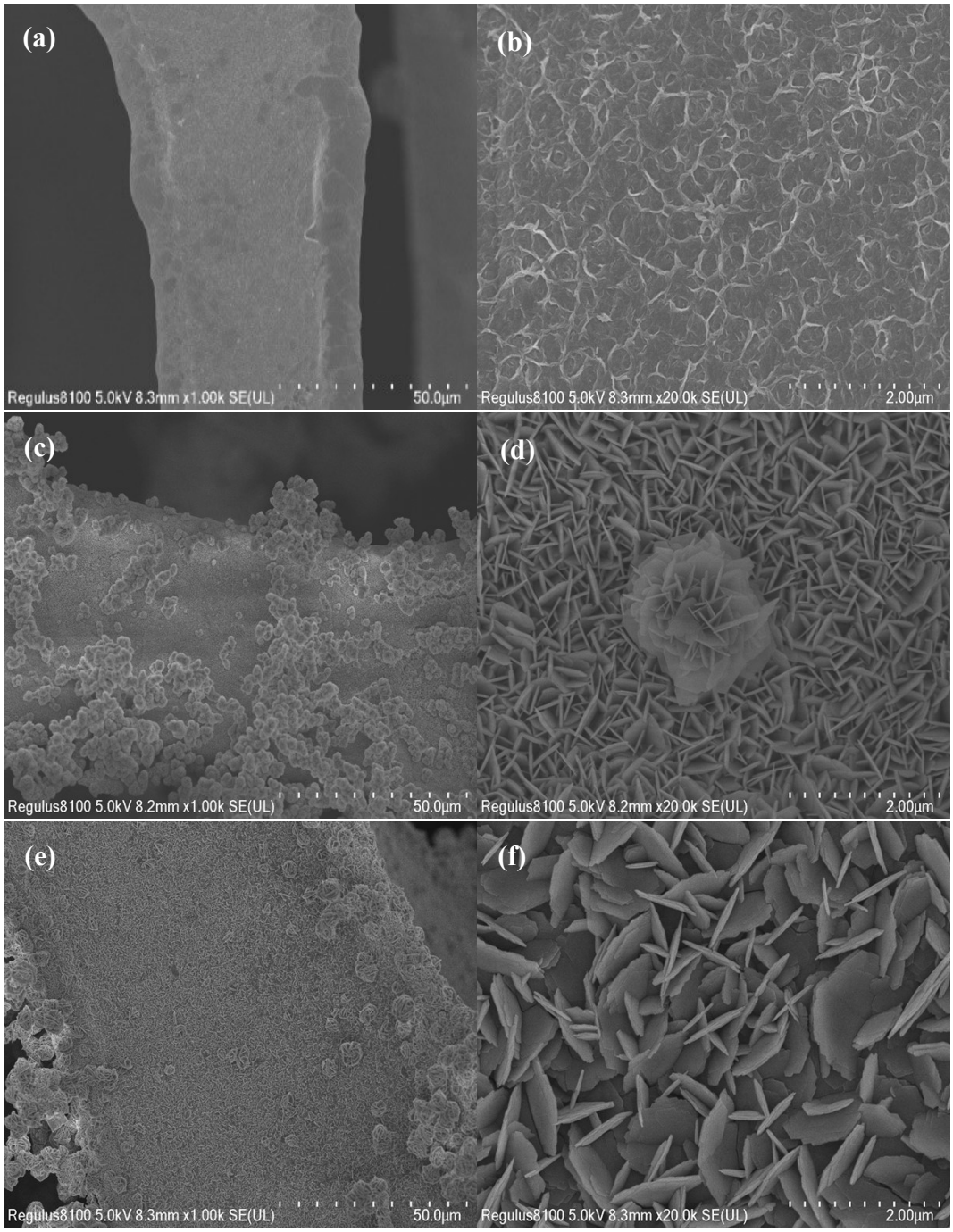

Figure S2. SEM images of (a-b) NF, (c-d) NiFe-LDHs, (e-f) NiCo-LDHs.

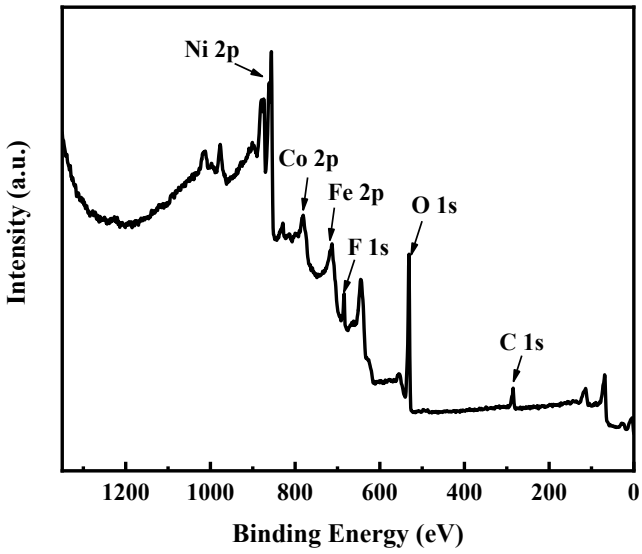

Figure S3. XPS survey spectra of NiFeCo-LDHs.

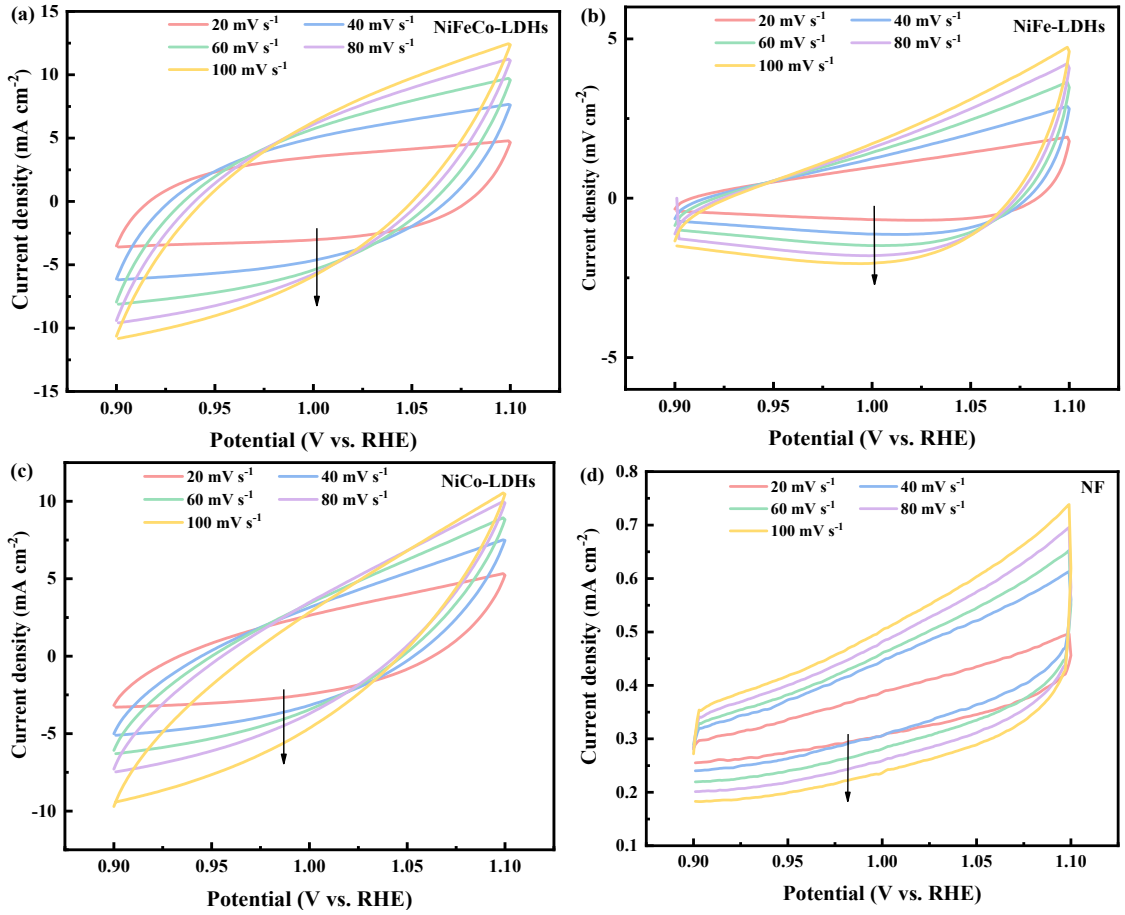

Figure S4. Cyclic voltammetry curves for materials on nickel foam (NF) for scanning rates (20, 40, 60, 80, 100 mV s^{-1}): (a) NiFeCo-LDHs, (b) NiFe-LDHs, (c) NiCo-LDHs, (d) NF.

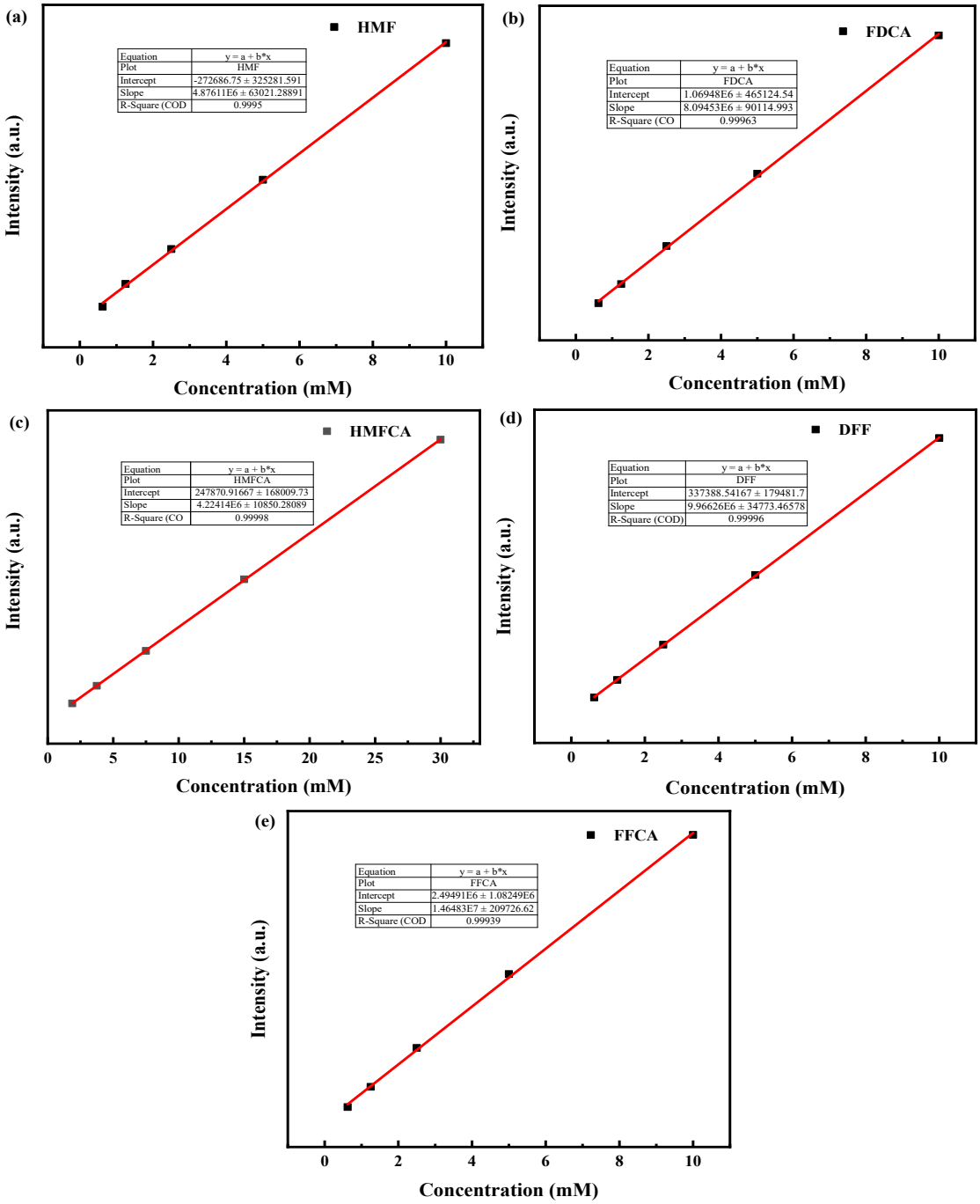

Figure S5. Standard lines of (a) HMF, (b) FDCA, (c) HMFCA, (d) DFF and (e) FFCA; (f) distribution of the products during reaction process.

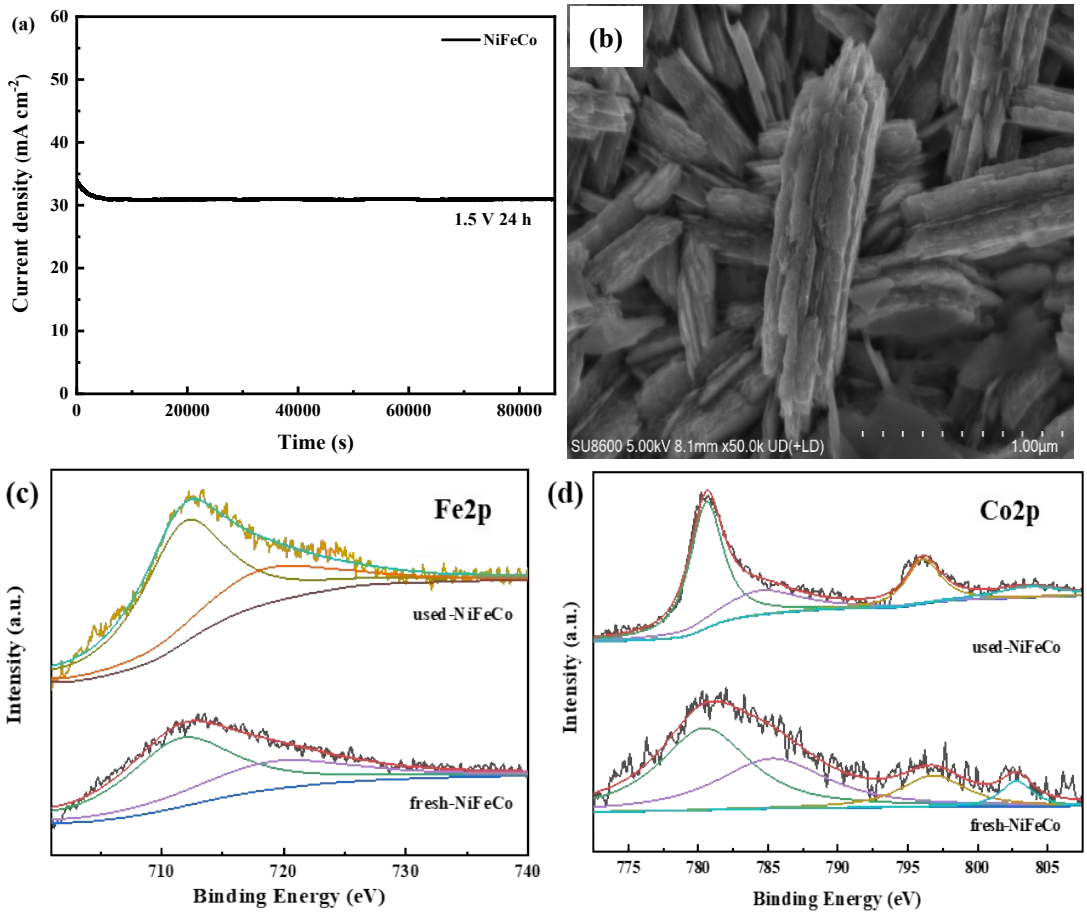

Figure S6. I-t curves (a) and SEM image of used-NiFeCo-LDHs (b), Morphological and valence changes in NiFeCo-LDHs electrode after electrocatalytic oxidation of HMF: (c) Fe 2p XPS spectra and (d) Co 2p XPS spectra.

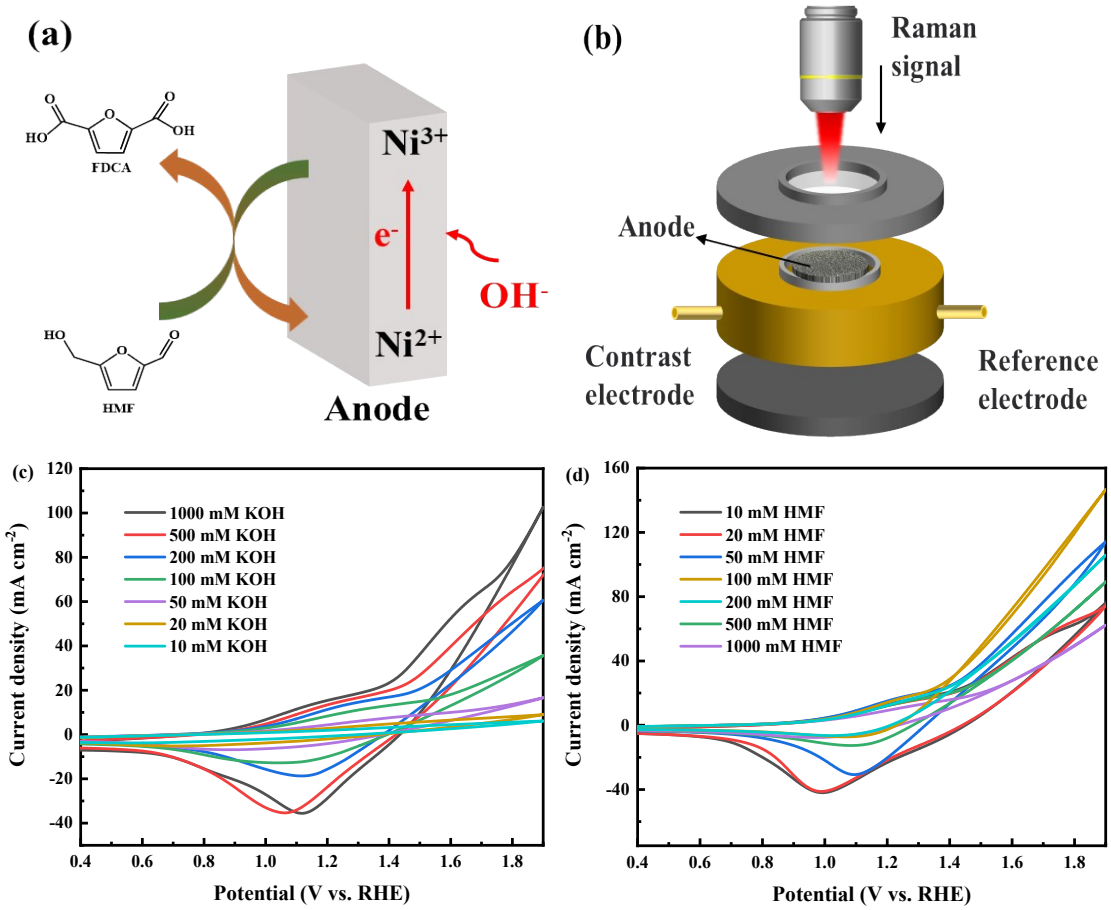

Figure S7. Scheme of HMFOR mechanism in NiFeCo-LDHs electrode (a), schematic diagram of in-situ electrochemical Raman test (b), the CV curves in 20 mM HMF with different concentrations of KOH (c) and in 1 M KOH for a range of HMF concentrations (d).

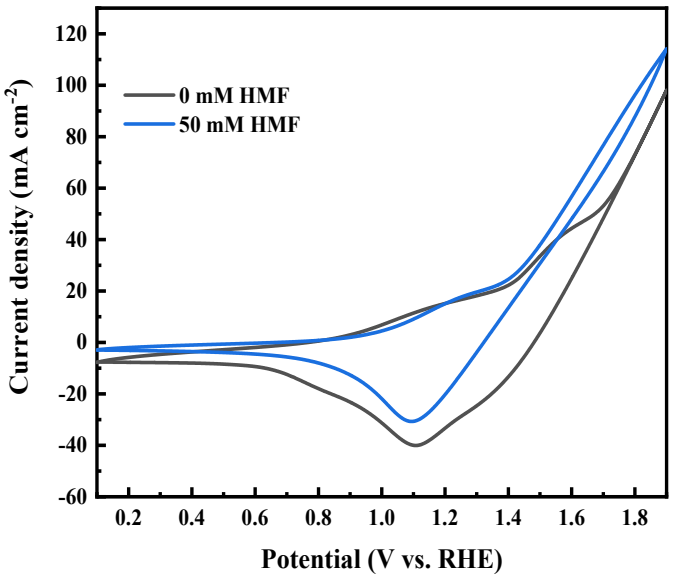

Figure S8. CV curves of 1 M KOH with and without 50 mM HMF.

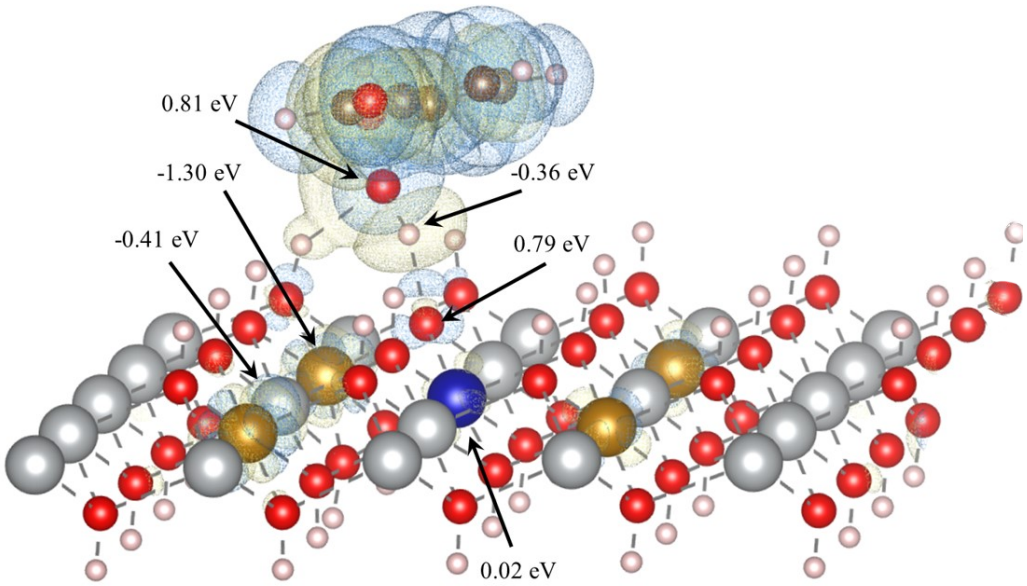

Figure S9. Charge density difference for HMF adsorption on NiFeCoOHO.

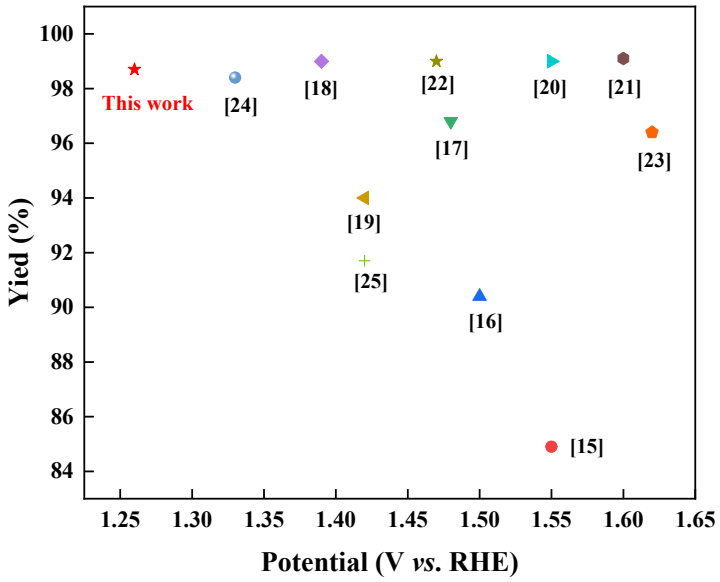

Figure S10. Performance of electrocatalysts. (A transition metal-based electrocatalyst in a recent electrocatalytic oxidation of HMF is included in the figure).

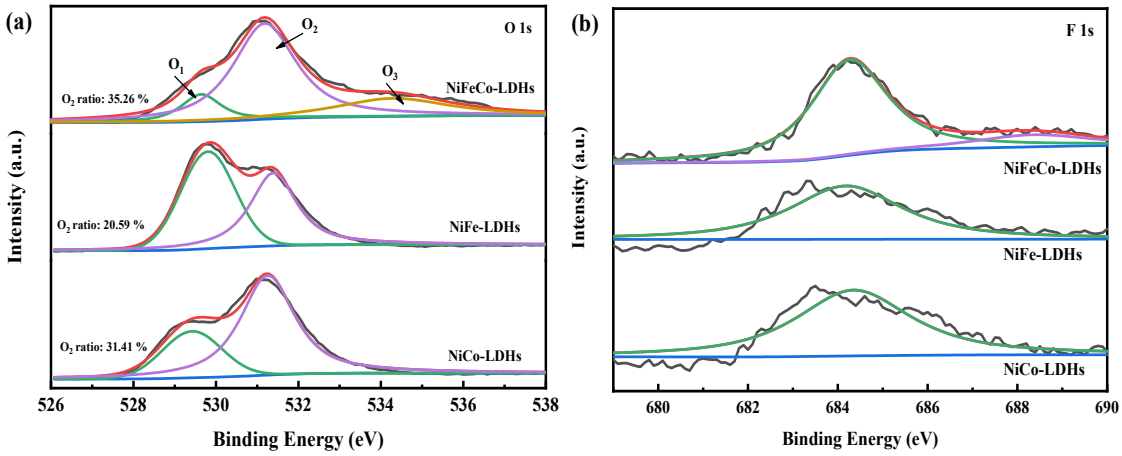

Figure. S11 XPS spectra of O 1s of catalysts.

Table. S1. Specific surface area, pore volume, and pore size of prepared catalysts.

Sample	BET surface area (m^2/g)	Micropore volume [a] (cm^3/g)	Mesopore volume [b] (cm^3/g)	Micropore size [a] (nm)	Mesopore size [b] (nm)
NiFeCo-LDHs	26.3	0.078	0.33	0.53	18.35
NiFe-LDHs	15.82	0.074	0.22	0.54	12.1
NiCo-LDHs	20.1	0.103	0.25	0.54	7.43

a: Calculated with Horvath-Kawazoe model

b: Calculated with BJH model.

Table S2. Ni content of prepared catalysts.

Catalyst	Ni content (%)	Oxygen vacancy (%)
NiFeCo-LDHs	19.7	35.26
NiFe-LDHs	14.8	20.59
NiCo-LDHs	15.4	31.41

Table S3. Oxygen evolution reaction (OER) performance of NiFeCo-LDHs electrocatalyst and literature electrocatalysts.

Catalyst	Electrolyte	Overpotential (mV) (@10 mA cm^{-1})	Ref.
NiFeCo-LDHs	1 M KOH	157	This work
$NiMoO_4$(0.5Fe)	1 M KOH	208	[10]
0.5Mo-$NiCo_2O_4$	3 M KOH	280	[11]
Ni@NCS-800	1 M KOH	330	[12]
Fe-Ni_2B/NF-x	1 M KOH	194	[13]
Ni-CNFs/Ir-$Co(OH)_2$	1 M KOH	240	[14]

Table S4. Comparison of catalytic activity of various materials for HMF oxidation to FDCA.

Electrode	Electrolyte	Potential (V *vs*. RHE)	HMF conversion (%)	FDCA yield (%)	FE (%)	Ref.
NiFeCo-LDHs	1 M KOH	1.26	100	98.7	98	This work
NiFe-LDHs	1 M NaOH	1.55	95.5	84.9	~90	[15]
$NiCo_2O_4$	1 M KOH	1.50	99.6	90.4	87.5	[16]
d-NiFe LDH/CP	1 M KOH	1.48	97.35	96.8	84.47	[17]
NiFeCoS-MOF	1 M KOH	1.39	100	99	99	[18]
CoFe PBA	1 M KOH	1.42	-	94	94	[19]
NiCoBDC-NF	1 M KOH	1.55	100	99	78.8	[20]
Ni-PA	1 M KOH	1.6	100	99.1	90	[21]
$Ni(OH)_2$/NF	1 M KOH	1.47	99.5	99	96	[22]
NCF	0.1M KOH	1.62	100	96.4	95	[23]
$CuMn_2O_4$	1 M KOH	1.33	100	98.4	96	[24]
NiCoMn-LDHs	1 M NaOH	1.42	100	91.7	90	[25]

References:

1. S. Yang, X. Xiang, Z. He, W. Zhong, C. Jia, Z. Gong, N. Zhang, S. Zhao and Y. Chen, *Chemical Engineering Journal*, 2023, **457**, 141344.
2. E. Cossar, M. S. E. Houache, Z. Zhang and E. A. Baranova, *Journal of Electroanalytical Chemistry*, 2020, **870**, 114246.
3. G. Kresse and J. Furthmuller, *Physical Review B*, 1996, **54**, 11169-11186.
4. G. Kresse and J. Furthmuller, *Computational Materials Science*, 1996, **6**, 15-50.
5. J. P. Perdew, K. Burke and M. Ernzerhof, *Physical Review Letters*, 1998, **80**, 891-891.
6. A. J. Tkalych, K. Yu and E. A. Carter, *Journal of Physical Chemistry C*, 2015, **119**, 24315-24322.
7. D. Sheppard, R. Terrell and G. Henkelman, *Journal of Chemical Physics*, 2008, **128**, 4106.
8. M. J. Eslamibidgoli, A. Gross and M. Eikerling, *Physical Chemistry Chemical Physics*, 2017, **19**, 22659-22669.
9. B. Zhou, Y. Li, Y. Zou, W. Chen, W. Zhou, M. Song, Y. Wu, Y. Lu, J. Liu, Y. Wang and S. Wang, *Angewandte Chemie-International Edition*, 2021, **60**, 22908-22914.
10. H. Hao, Y. Li, Y. Wu, Z. Wang, M. Yuan, J. Miao, Z. Lv, L. Xu and B. Wei, *Materials Today Energy*, 2022, **23**.
11. S. Xiong, L. Wang, H. Chai, Y. Xu, Y. Jiao and J. Chen, *Journal of Colloid and*

Interface Science, 2022, **606**, 1695-1706.

12. K. B. Patel, B. Parmar, K. Ravi, R. Patidar, G. R. Bhadu, J. C. Chaudhari and D. N. Srivastava, *Applied Surface Science*, 2023, **616**, 156499.
13. Y. Zhang, H. Xu and S. Ma, *Dalton Transactions*, 2023, **52**, 9077-9083.
14. J. Xu, S. Cao, M. Zhong, X. Chen, W. Li, S. Yan, C. Wang, Z. Wang, X. Lu and X. Lu, *Separation and Purification Technology*, 2023, **324**, 124638.
15. M. Zhang, Y. Liu, B. Liu, Z. Chen, H. Xu and K. Yan, *ACS Catalysis*, 2020, **10**, 5179-5189.
16. M. J. Kang, H. Park, J. Jegal, S. Y. Hwang, Y. S. Kang and H. G. Cha, *Applied Catalysis B-Environmental*, 2019, **242**, 85-91.
17. Y.-F. Qi, K.-Y. Wang, Y. Sun, J. Wang and C. Wang, *ACS Sustainable Chemistry & Engineering*, 2022, **10**, 645-654.
18. Y. Feng, K. Yang, R. L. L. Smith Jr and X. Qi, *Journal of Materials Chemistry A*, 2023, **11**, 6375-6383.
19. W. Hadinata Lie, C. Deng, Y. Yang, C. Tsounis, K.-H. Wu, M. V. Chandra Hioe, N. M. Bedford and D.-W. Wang, *Green Chemistry*, 2021, **23**, 4333-4337.
20. Y. Song, Z. Li, K. Fan, Z. Ren, W. Xie, Y. Yang, M. Shao and M. Wei, *Applied Catalysis B-Environment and Energy*, 2021, **299**, 120669.
21. S. Liu, X. Yuan, X. Huang, Y. Huang, C. Sun, K. Qian and W. Zhang, *Frontiers in Chemistry*, 2023, **11**.
22. G. Yang, X. Mu, Y. Jin, T. Fan, S. Wang, F. Yuan and J. Ma, *Applied Surface*

Science, 2022, **594**.

23. D.-H. Nam, B. J. Taitt and K.-S. Choi, *Acs Catalysis*, 2018, **8**, 1197-1206.

24. B. Zhu, Y. Qin, J. Du, F. Zhang and X. Lei, *Acs Sustainable Chemistry & Engineering*, 2021, **9**, 11790-11797.

25. B. Liu, S. Xu, M. Zhang, X. Li, D. Decarolis, Y. Liu, Y. Wang, E. K. Gibson, C. R. A. Catlow and K. Yan, *Green Chemistry*, 2021, **23**, 4034-4043.